Peer-reviewed version available at Appl. Sci. 2019, 9, 3991; doi:10.3390/app9193991

Article

Near-field IR orientational spectroscopy of silk

Meguya Ryu[1], Reo Honda[1], Aina Reich[2], Adrian Cernescu[2], Jing-Liang Li[3], Jingwen Hu[4,5], Saulius Juodkazis[4,5,6]*, and Junko Morikawa[1,6]*

1 School of Materials and Chemical Technology, Tokyo Institute of Technology, 2-12-1, Ookayama, Meguro-ku, Tokyo 152-8550, Japan
2 Neaspec GmbH, Bunsenstrasse 5, 82152 Martinsried, Germany
3 Institute for Frontier Materials, Deakin University, Geelong, Vic 3220, Australia
4 Swinburne University of Technology, John st., Hawthorn, 3122 Vic, Australia
5 Melbourne Center for Nanofabrication, Australian National Fabrication Facility, Clayton 3168, Melbourne, Australia
6 Tokyo Tech World Research Hub Initiative (WRHI), School of Materials and Chemical Technology, Tokyo Institute of Technology, 2-12-1, Ookayama, Meguro-ku, Tokyo 152-8550, Japan

Abstract: Orientational dependence of the IR absorbing amide bands of silk is demonstrated from two orthogonal longitudinal and transverse microtome slices only $\sim$ 100 nm thick. A scanning near-field optical microscopy (SNOM) which preferentially probes orientation perpendicular to the sample's surface was used. Spatial resolution of silk-epoxy boundary was defined with a $\sim$ 100 nm resolution while the spectra were collected by a $\sim$ 10 nm tip. Ratio of the absorbance of the amide-II C-N at 1512 cm^{-1} and amide-I C=O β-sheets at 1628 cm^{-1} showed sensitivity of SNOM to the molecular orientation. SNOM characterisation is complimentary to the far-field absorbance which is sensitive to the in-plane polarisation. Volumes with cross sections smaller than 100 nm can be characterised for molecular orientation. A method of absorbance measurements at four angles of slice cut orientation, which is equivalent to the four polarisation angles absorbance measurement is proposed.

Keywords: silk; anisotropy; absorbance; retardance

1. Introduction

Nanofabrication with few nanometers resolution now become routine using electron emission [1] and thermal probes [2,3]. Structuring of materials with nanoscale precision requires an equally matching characterisation capabilities. Structural anisotropy of materials underpin their optical, thermal, mechanical properties and have to be determined at the highest transverse and longitudinal resolutions [4,5]. For example, the fibril of tens-of-nanometers in silk defines its thermal properties [6]. Comparable IR absorbance spectra of silk were obtained using three different methods [7]: *(i)* a table-top Fourier transform infrared (FTIR) transmission, *(ii)* a synchrotron-based attenuated total reflection (ATR) FTIR, and *(iii)* an atomic force microscopy (AFM) tip response to the IR absorbed light, also known as nano-IR [8]. The AFM-based nano-IR technique acquires structural information at the nanoscale, the area under the AFM tip from volume with lateral cross-section of $\sim$ 20 nm. Different sensitivity of reflectance R and absorbance A to the real and imaginary parts of refractive index $\tilde{n} = n + i\kappa$ becomes important. The far-field absorbance is defined by κ, while the near-field ATR-FTIR mode is affected by n due to the Snell's law [9,10]. Another tip-based near-field optical charactrisation technique - scanning near-field optical microscopy (SNOM) - is a popular method to map surface topography and refractive index $\tilde{n}$ decoupled from the scattered light. Typically, a p-polarised light with E-field aligned with the tip and perpendicular to the probed surface defines the strongest coupling and the field enhancement. Noteworthy, this E-field component is absent in the

Preprints (www.preprints.org) | NOT PEER-REVIEWED | Posted: 1 September 2019 doi:10.20944/preprints201909.0013.v1

Peer-reviewed version available at Appl. Sci. 2019, 9, 3991; doi:10.3390/app9193991

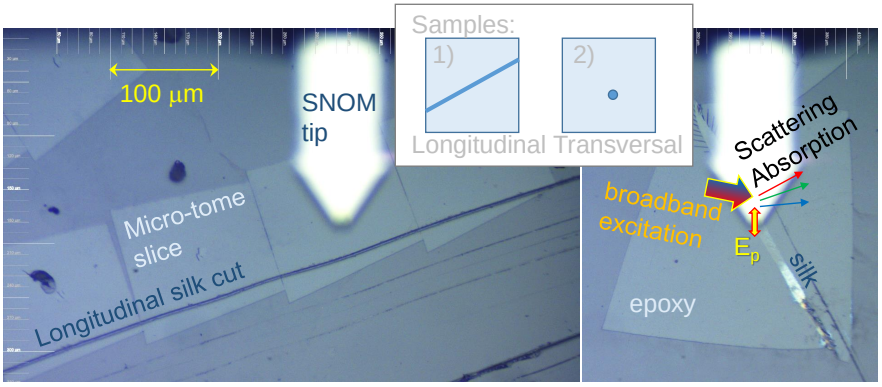

Figure 1. Optical image of longitudinal micro-tome slices of *Bombyx mori* fibers. Left image shows schematically the principle of spectrally broadband excitation and detection of scattered light implemented in neaspec tool for detection of nanoscale absorbance and scattering. The excitation light field is p-polarised, E_p.

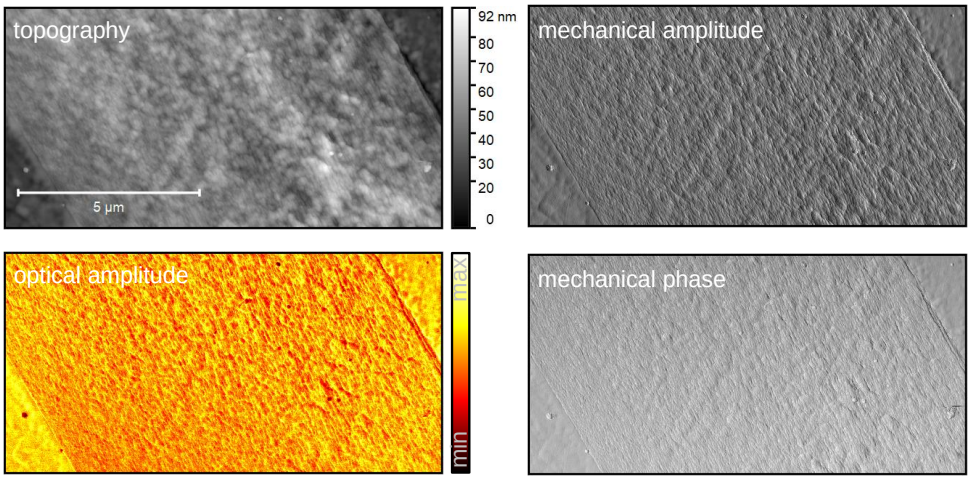

Figure 2. Raw SNOM (neaspec) data from a longitudinal slice of *Bombyx mori* silk: topography (height: 0 - 92 nm), mechanical amplitude and phase, and optical amplitude (proportional to the reflectivity integrated over 1300-2020 cm^{-1}) IR spectral range.

paraxial geometry used for transmission measurements; it only becomes present under the most tight optical focusing conditions. SNOM, allows to probe material with E-field normal to the surface and was used in this study to test orientational sensitivity of this method to alignment of amide bands in silk sliced along and across the fiber.

Here, we used scattering SNOM to probe n, κ and to determine spectral differences due to orientation in the absorbance at the amide bands of silk fibers. Cross-sections of silk fibers were prepared using ultramicrotome. Silk was chosen due to its well known spectral properties and uniaxial symmetry which can be examined from longitudinal and transverse microtome slices [6]. Sub-wavelength resolutions in hyperspectral IR mapping of absorbance and orientational properties of the absorption bands were measured from 100-nm-thick slices of silk.

Preprints (www.preprints.org) | NOT PEER-REVIEWED | Posted: 1 September 2019 doi:10.20944/preprints201909.0013.v1

Peer-reviewed version available at Appl. Sci. 2019, 9, 3991; doi:10.3390/app9193991

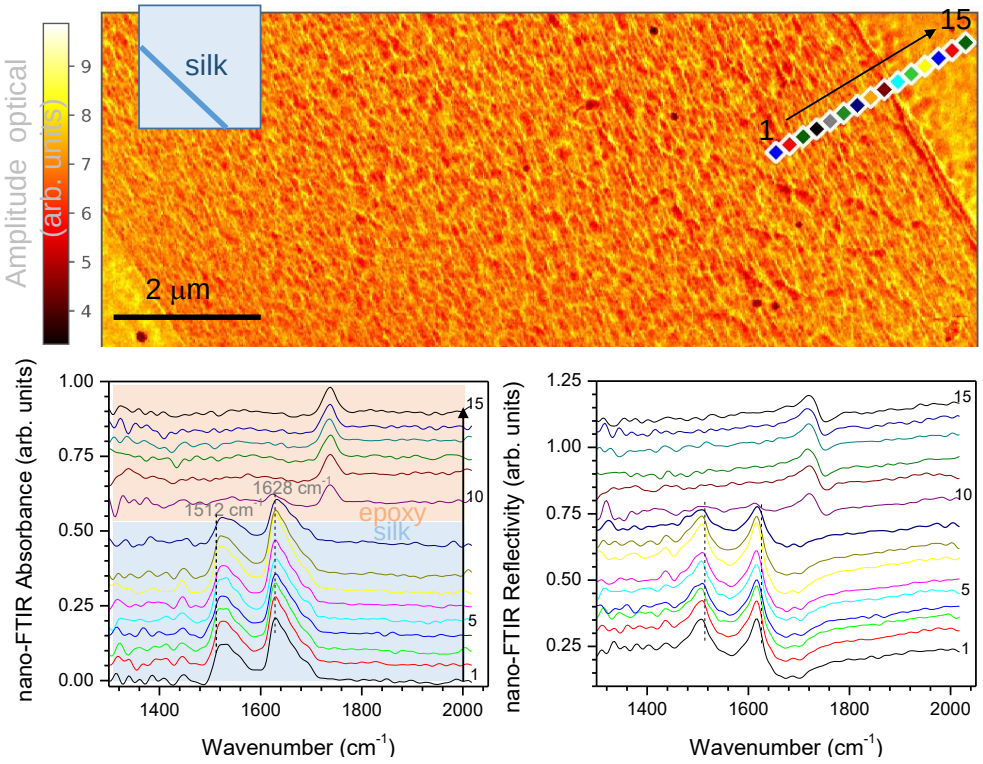

Figure 3. Scattering SNOM mapping and point spectra at 15 locations separated on a line by 200 nm (color marked) measured on the longitudinal slice. The amplitude and phase of the measured spectra.

2. Methods and samples

2.1. Silk slices

Preparation of white silk *Bombyx mori* fibers was the same as described previously [12]. In short, the cocoons were boiled three times in an aqueous 0.5% (w/v) Na_2CO_3 solution to remove the sericin. The degummed silk fibers were rinsed with warm ultra pure water at 60°C thoroughly to remove the residual sercin and dried at room temperature.

Silk fibers were embedded in epoxy resin (Oken Ltd., Japan) and thin-sectioned by ultramicrotomy to achieve a sample thickness of $\sim$ 100 nm. Slices were then immobilised on a gold mirror for measurements.

2.2. IR spectral measurements

The sub-diffraction scattering (s-)SNOM (neaspec GmbH) uses a metalised AFM tip which maps the surface relief (topography) by its basic AFM operation, and simultaneously, under external IR illumination (broadband laser working by difference-frequency generation, Toptica), acts as a light-concentrating antenna such that the sample is probed with a nanofocused light field. The AFM tapping mode operation (ca. 60 nm amplitude) modulates the near-field interaction between the tip and sample [13]. The measured nano-IR absorbance is proportional to the imaginary part of the scattering coefficient $\sigma_n(\omega) = s(\omega)e^{i\phi(\omega)}$, which relates the light scattered field $E_s(\omega)$, and the incident field $E_i(\omega)$ through the equation $E_s = \sigma_n E_i$, where $s(\omega)$ and $\phi(\omega)$ are the amplitude and phase of the back-scattered spectra [10]. Using the asymmetric Michelson interferometer, the full complex function of the scattered optical signal can be recorded, therefore enabling the simultaneous measurement of both nano-IR absorbance and reflectivity spectra [10]. The Michelson interferometer and a lock-in detection of the signal at higher harmonic of the tapping frequency $\sim$250 kHz provides

Preprints (www.preprints.org) | NOT PEER-REVIEWED | Posted: 1 September 2019 doi:10.20944/preprints201909.0013.v1

Peer-reviewed version available at Appl. Sci. 2019, 9, 3991; doi:10.3390/app9193991

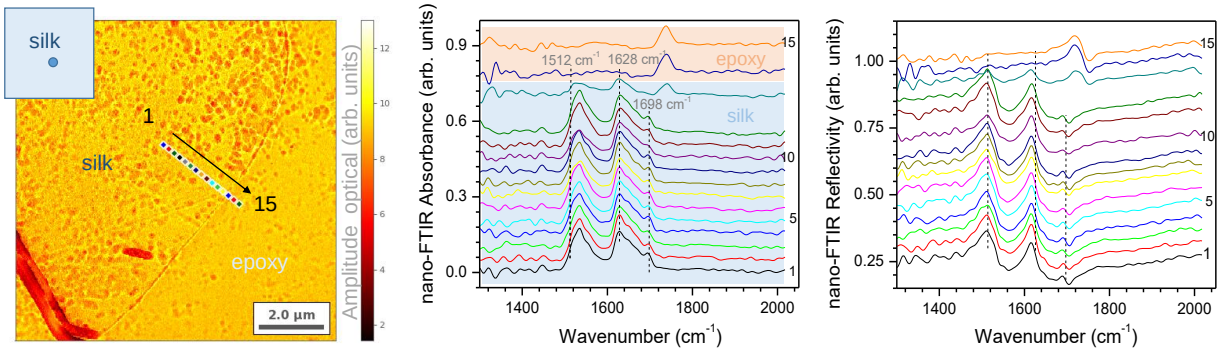

Figure 4. Transverse slice of silk. SNOM map and the amplitude and phase of scattered field at 15 equidistant points across the silk-epoxy boundary.

background-free nano-IR spectra and images with maximum resolution imposed by the AFM tip size independent of the laser wavelength [10].

The nano-FTIR spectra were recorded in ∼100 s/spectrum with a spectral resolution of 10 cm^{-1}. Removal of the instrumental response function from the nano-FTIR spectra was done by normalization of the measured spectra to a reference Si signal. Resulting nano-FTIR absorbance and reflectivity spectra are directly correlated with the standard far-field IR spectra [14,15].

3. Results and discussion

Dimensions of crystalline β-sheet fibrils in silk fibers is $\simeq$ 10 nm [16]. SNOM measurements are well suited to measure n and κ from areas of comparable dimensions [12]. Whether it is possible to determine optical anisotropy due to molecular orientation using a point-like excitation source was the motivation of this study. If the anisotropy of absorbance (dichroism $\Delta\alpha \propto \Delta\kappa$) and refractive index (birefringence Δn) could be measured with a point-like source with s-SNOM, this would open possibility to determine anisotropy and molecular orientation at the highest sub-wavelength resolution at nanoscale.

The birefringence originates from alignment of molecular bonds or secondary ordering and can be detected at different spectral ranges [17]. Molecular alignment of the amide-II at 1512 cm^{-1} (C-N) and amide-I β-sheets at 1628 cm^{-1} (C=O) was measured form micron-thick longitudinal silk slices [11]. In-plane perpendicular orientation between C=O and C-N bonds was revealed [11] using a longitudinal slice of silk fiber, which facilitated fidelity of measurements due to uniformity of thickness [18].

In this study s-SNOM data were collected at the IR spectral range together with topography map (Fig. 2). The mechanical amplitude and phase are related to the stability of the feedback loop and were used as an qualitative error signal, i.e., unexpected changes in the mechanical amplitude correlated with errors in the near-field amplitude. The optical amplitude map is also shown (Fig. 2) and is dominated by the reflectivity $\propto n$ of the surface, which is usually very low for the polymers (emissivity $\propto \kappa$ is high at the absorption bands). Both, mechanical and optical mapping revealed a clear boundary between the longitudinal silk fiber slice and surrounding epoxy (Fig. 2). Recently, it was demonstrated that mechanical viscoelastic parameters: the Young's modulus, viscosity coefficient, and retardation time can be determined using the amplitude modulated-frequency modulated (AM-FM) mode of cantilever response [19] and are linked to the topography of the sample via the offset of the tapping mode signal.

The amide I and II bands [12] were well recognisable in the nano-FTIR absorbance spectra collected from different single measurements points (Fig. 2). Measurements were made along 3 μm

Preprints (www.preprints.org) | NOT PEER-REVIEWED | Posted: 1 September 2019 doi:10.20944/preprints201909.0013.v1

Peer-reviewed version available at Appl. Sci. 2019, 9, 3991; doi:10.3390/app9193991

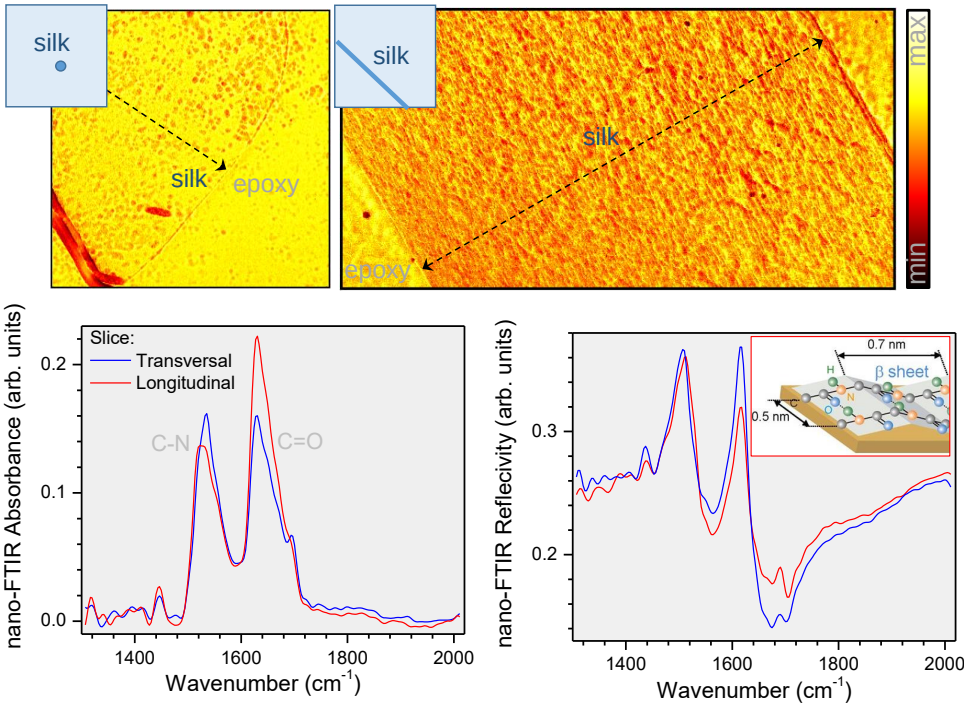

Figure 5. SNOM maps of the transverse and longitudinal silk slices together with averaged nano-FTIR absorbance and reflectance spectra. Inset in reflectivity panel shows a molecular orientation of the amide-I,II bands in β-sheet crystalline regions for the longitudinal slice (adopted form ref. [11]). Note, chemical bonding in the β-sheets plane only is shown; the C=O bonds have a radial distribution along the fiber direction and their second order momentum distribution was determined in Supplement of ref. [11].

linear scan with separation of 200 nm between the measurement sites. Clear transition from the silk to epoxy was observed and a half-step can be defined as the upper bound of the resolution.

Transverse silk slice showed similar topography and mechanical (amplitude and phase) mapping with a slightly larger reflectivity (Fig. 4). The same scan along the line showed a distinct transition from silk to epoxy. The dark regions along the boundary were observed with spectral features mixed between silk and epoxy (Fig. 4). Since the 100 nm thickness of the slice was only approximately twice larger than the diameter of the fiber, mechanical cracks were expected under sheer forces applied during slicing.

Comparison of spectra measured from transverse and longitudinal slices is shown in Fig. 5. Different ratio of the amide-II and I bands is directly related to the orientation as we showed by the far-field absorbance [11]. For the longitudinal slice, C=O (amide-I) is radially distributed and the most strongly coupled to the E_p of the SNOM needle while C-N (amide-II) is perpendicular to the SNOM tip, hence, uncoupled to the absorbing dipole. The inset in the reflectivity spectum (Fig. 5) shows mutually perpendicular in-plane orientations of the C=O and C-N amide bands on the longitudinal slice; note, the C=O is radially distributed if observed out-of-plane. This illustration also clarifies that for the transverse slice $E_p \parallel$(C-N) and perpendicular $E_p \perp$(C=O). The two transverse and longitudinal slices represents two cases when E_p is most strongly coupled to one or the other amide bands. The different ratio of the heights of the two amide absorbance peaks (Fig. 5) is directly related to the different orientation as we observed in the far-field measurements [11]. Also, observation of a side-lobe peak at 1698 cm^{-1} is related to the β-sheet amide [11] and was only observed in the transverse slice (Fig. 4).

This first qualitative result shows that it is feasible to detect orientational difference in molecular alignment from single point measurement using tip source of excitation. Further efforts should be concentrated to develop near-field four-polarisation analogy of orientation mapping (Fig. 6) which

Preprints (www.preprints.org) | NOT PEER-REVIEWED | Posted: 1 September 2019 doi:10.20944/preprints201909.0013.v1

Peer-reviewed version available at Appl. Sci. 2019, 9, 3991; doi:10.3390/app9193991

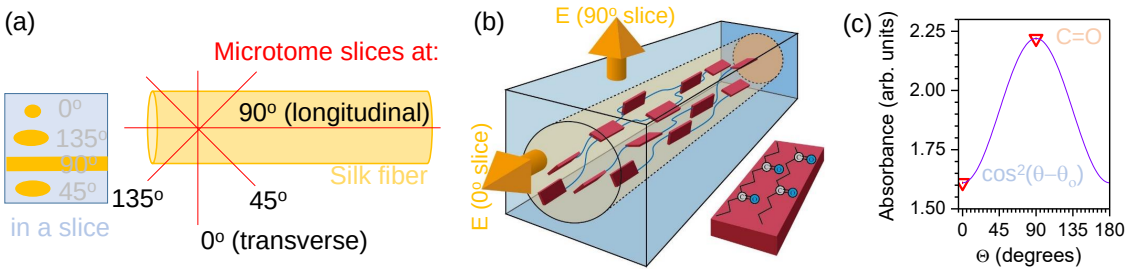

Figure 6. (a) Concept of four-angle absorbance measurements where instead of polarisation, four different orientation micro-tome slices are prepared. In this study we carried out measurements on two 90° and 0° longitudinal and transverse slices, respectively. (b) Visualisation of the a silk fiber with its internal β-sheet structure. (c) Orientation determination of C=O β-sheet absorbers at 1628 cm^{-1} using different orientation slices (data markets for the transverse $\theta = 0°$ and longitudinal $\theta = 90°$ data) microtome slices; θ_o is the initial orientation. Note, for quantitative determination of orientation, four orientation slices are required.

for absorbance has been developed for the far field [20]. As demonstrated recently, the orientational dependence of transmittance/absorbance can be used to separate contributions due to the real and imaginary parts of refractive index [21]. Birefringence and dichroism, which both are orientation dependent can be separated by four-angle absorbance method [21]. Here we show that similar concept of four-angle method but for the orientation of microtome cuts should provide orientation of the absorbers in the sample for the E-field perpendicular to the sample's surface (SNOM geometry) as illustrated in Fig. 6(c). A structural knowledge of molecular alignment usually obtained by X-ray diffraction (XRD), could be obtained by a direct near-field measurements with resolution down to tens-of-nm (Fig. 6(b)); a cartoon version of β-sheet is shown where the Oxygens are orientated out of plane.

4. Conclusions and outlook

In summary, spectral characterisation, lateral mapping of nano-IR absorbance and reflectance with deep sub-wavelength resolution at IR molecular finger printing spectral window were demonstrated using thin 100 nm transverse and longitudinal slices of silk. Hyper-spectral mapping across the silk fiber slice was obtained at a high accuracy and reproducibility. Possibility of orientational measurements using SNOM tip is proposed and demonstrated at two angles (two slices of silk fiber) using the amide bands and previously measured far-field IR spectra. Since preparation of thin micro-tome slices of soft bio-materials is not altering their structure [12], it opens a possibility to read optical properties from nano-volumes prepared by careful alignment of microtome cuts. One can envisage that using slices of silk fiber at different angles 0° (transverse), ±45°, and 90° (longitudinal), the four-orientation mapping equivalent to the four-polarisation method [20] can be developed and will be focus of future study. Measurement of orientational changes in the regions of laser-induced material modification by re-melting [22], phase change and ablation [23] will benefit form the introduced method.

Author Contributions: Conceptualization, J. M., M. R., S.J.; methodology, M.R., J.M., A.C.; experiments and sample preparation, M.R., R.H., A.R., J.H., J.-L.L.; data analysis, all the authors; writing–review and editing, all the authors.

Funding: This research was funded by JSPS KAKENHI Grants No.16K06768, 18H04506 (Japan) and the Australian Research Council Discovery projects DP1901032.

Acknowledgments: We are grateful for R. Kikuchi from Materials Analysis Division of Tokyo Institute of Technology, Ookayama, for his assistance with ultramicrotomy. SJ is grateful for sabbatical stays at Tokyo Institute of Technology and Shizuoka University in 2018.

Conflicts of Interest: The authors declare no conflict of interest.

References

1. Rangelow, I.W.; Ahmad, A.; Ivanov, T.; Kaestner, M.; Krivoshapkina, Y.; Angelov, T.; Lenk, S.; Lenk, C.; Ishchuk, V.; Hofmann, M.; Nechepurenko, D.; Atanasov, I.; Volland, B.; Guliyev, E.; Durrani, Z.; Jones, M.; Wang, C.; .; Liu, D.; Reum, A.; Holz, M.; Nikolov, N.; Majstrzyk, W.; Gotszalk, T.; Staaks, D.; Dallorto, S.; Olynick, D.L. Pattern-generation and pattern-transfer for single-digit nano devices. *J Vac Sci Techn B* **2016**, *34*, 06K202.
2. Paul, P.C.; Knoll, A.W.; Holzner, F.; Despont, M.; rig, U.D. Rapid turnaround scanning probe nanolithography. *Nanotechnology* **2011**, *22*, 275306.
3. Holzner, F.; Paul, P.; Drechsler, U.; Despont, M.; Knoll, A.W.; Duerig, U. High density multi-level recording for archival data preservation. *Appl. Phys. Lett.* **2011**, *99*, 023110.
4. Shao, Z.; Vollrath, F. Surprising strength of silkworm silk. *Nature* **2002**, *418*, 741.
5. Jiang, J.; Zhang, S.; Qian, Z.; Qin, N.; Song, W.; Sun, L.; Zhou, Z.; Shi, Z.; Chen, L.; Li, X.; Mao, Y.; Kaplan, D.L.; Corder, S.; Chen, X.; Liu, M.; Omenetto, F.G.; Xia, X.; Tao, T.H. Protein Bricks: 2D and 3D Bio-Nanostructures with Shape and Function on Demand. *Adv. Mat.* **2002**, *30*, 1705919.
6. Choi, S.H.; Kim, S.W.; Ku, Z.; Visbal-Onufrak, M.A.; Kim, S.R.; Choi, K.H.; Ko, H.; Choi, W.; Urbas, A.M.; Goo, T.W.; Kim, Y.L. Anderson light localization in biological nanostructures of native silk. *Nature Communicaitons* **2018**, *9*, 452.
7. Ryu, M.; Kobayashi, H.; Balčytis, A.; Wang, X.; Vongsvivut, J.; Li, J.; Urayama, N.; Mizeikis, V.; Tobin, M.; Juodkazis, S.; Morikawa, J. Nanoscale chemical mapping of laser-solubilized silk. *Mat. Res. Express* **2017**, *4*, 115028.
8. Dazzi, A.; Prazeres, R.; Glotin, F.; Ortega, J.M. Local infrared microspectroscopy with subwavelength spatial resolution with an atomic force microscope tip used as a photothermal sensor. *Opt. Lett.* **2005**, *30*, 2388 – 2390.
9. Bertie, E.; Michaelian, K.H. Comparison of infrared and Raman wave numbers of neat molecular liquids: which is the correct infrared wavenumber to use? *J. Chem. Phys.* **1998**, *109*, 6764 – 6771.
10. Huth, F.; Schnell, M.; Wittborn, J.; Ocelic, N.; Hillenbrand, R. Infrared-spectroscopic nanoimaging with a thermal source. *Nature Materials* **2011**, *10*, 352–356.
11. Ryu, M.; Bačytis, A.; Wang, X.; Vongsvivut, J.; Hikima, Y.; Li, J.; Tobin, M.J.; Juodkazis, S.; Morikawa, J. Orientational Mapping Augmented Sub-Wavelength Hyper-Spectral Imaging of Silk. *Sci. Reports* **2017**, *7*, 7419.
12. Ryu, M.; Honda, R.; Cernescu, A.; Vailionis, A.; Balčytis, A.; Vongsvivut, J.; Li, J.; Linklater, D.; Ivanova, E.; Mizeikis, V.; Tobin, M.; Morikawa, J.; Juodkazis, S. Nanoscale optical and structural characterisation of silk. *Beilstein J. Nanotechn.* **2019**, *10*, 922–929.
13. Keilmann, F.; Hillenbrand, R. Near-field microscopy by elastic light scattering from a tip. *Phil. Trans. R. Soc. Lond. A* **2004**, *362*, 787–805.
14. Huth, F.; Govyadinov, A.; Amarie, S.; Nuansing, W.; Keilmann, F.; Hillenbrand, R. Nano-FTIR Absorption Spectroscopy of Molecular Fingerprints at 20 nm Spatial Resolution. *Nano Lett.* **2012**, *12*, 3973–3978.
15. Westermeier, C.; Cernescu, A.; Amarie, S.; Liewald, C.; Keilmann, F.; Nickel, B. Sub-micron phase coexistence in small-molecule organic thin films revealed by infrared nano-imaging. *Nature Communications* **2014**, *5*, 4101.
16. Drummy, L.F.; Farmer, B.L.; Naik, R.R. Correlation of the β-sheet crystal size in silk fibers with the protein amino acid sequence. *Soft Matter* **2007**, *3*, 877–882.
17. Balčytis, A.; Ryu, M.; Wang, X.; Novelli, F.; Seniutinas, G.; Du, S.; Wang, X.; Li, J.; Davis, J.; Appadoo, D.; Morikawa, J.; Juodkazis, S. Silk: Optical Properties over 12.6 Octaves THz-IR-Visible-UV Range. *Materials* **2017**, *10*, 356.
18. Honda, R.; Ryu, M.; Li, J.L.; Mizeikis, V.; Juodkazis, S.; Morikawa, J. Simple multi-wavelength imaging of birefringence:case study of silk. *Sci. Reports* **2002**, *8*, 17652.
19. Benaglia, S.; Amo, C.A.; Garcia, R. Fast, quantitative and high resolution mapping of viscoelastic properties with bimodal AFM. *Nanoscale* **2019**, *11*, 15289 – 15297.
20. Hikima, Y.; Morikawa, J.; Hashimoto, T. FT-IR Image Processing Algorithms for In-Plane Orientation Function and Azimuth Angle of Uniaxially Drawn Polyethylene Composite Film. *Macromolecules* **2011**, *44*, 3950 – 3957.

21. Ryu, M.; Honda, R.; Balcytis, A.; Vongsvivut, J.; Tobin, M.; Juodkazis, S.; Morikawa, J. Hyperspectral mapping of anisotropy. *Nanoscale Horizons* **2019**, p. DOI:10.1039/C9NH00340A; online 23 July 2019.
22. Vanagas, E.; Kudryashov, I.; Tuzhilin, D.; Juodkazis, S.; Matsuo, S.; Misawa, H. Surface nanostructuring of borosilicate glass by femtosecond nJ energy pulses. *Appl. Phys. Lett.* **2003**, *82*, 2901–2903.
23. Yamasaki, K.; Juodkazis, S.; Matsuo, S.; Misawa, H. Three-dimensional microchannels in polymers: one step fabrication. *Appl. Phys. A* **2003**, *77*, 371–373.